Journal of Molecular Graphics and Modelling 44 (2013) 44–53

Contents lists available at ScienceDirect

Journal of Molecular Graphics and Modelling

journal homepage: www.elsevier.com/locate/JMGM

Quantum polarized ligand docking investigation to understand the significance of protonation states in histone deacetylase inhibitors

Subha Kalyaanamoorthy[a,b], Yi-Ping Phoebe Chen[a,*]

[a] Faculty of Science, Technology and Engineering, La Trobe University, Melbourne, Australia
[b] CSIRO Ecosystem Sciences, Canberra, ACT 2601, Australia

ARTICLE INFO

Article history:
Accepted 1 May 2013
Available online 14 May 2013

Keywords:
Protonation
Quantum mechanics/molecular mechanics
Quantum polarized ligand docking
Histone deacetylase inhibitors
Binding free energies
MM-GBSA

ABSTRACT

The effects of different protonation states of the hydroxamic acid (HA) inhibitors against the class I histone deacetylase enzymes (HDACs) have been studied using the state of the art quantum polarized ligand docking (QPLD) and molecular mechanics-generalized Born surface area (MM-GBSA) approaches. The binding modes of the inhibitors and their inter-molecular interactions with class I HDACs, in response to the protonation states of the inhibitors, are explored. Our results indicate that the different protonation states of the inhibitors exhibit significant differences in their interactions with the catalytic zinc metal ion and the other active site residues in the HDAC enzymes, which in turn affect the 'Histidine-Aspartate' charge relay mechanism. The QPLD calculations show that the protonated states of the inhibitors display higher scores in all the class I HDACs in this study, while the deprotonated forms present lower scores. The molecular electrostatic potentials and the other physico-chemical descriptors support the results. The MM-GBSA approach employed in the present work has been able to accurately calculate the relative binding free energies of the neutral and the protonated HA inhibitors; those were close to the experimental values. However, the MM-GBSA approach breaks down while calculating the binding free energies of the deprotonated inhibitors, which resulted in unrealistic values. Large energetic differences were found in the polar electrostatic solvation energy terms and the coulombic contributions in the deprotonated inhibitors. Thus improvements in the present solvation models and force fields become inevitable for the inclusions of charged states of inhibitors in computational drug discovery.

1. Introduction

Acetylation is one of the important post-translational modifications of histones, which is linked with early gene transcription [1]. Acetylation of histone tails is a reversible process that is mediated by the two counter-acting enzyme classes, histone acetyl transferases (HATs) and histone deacetylases (HDACs). HATs are involved in the acetylation of the ε-amino group of the lysine residues that are present in the N-terminal tails of the histone proteins, whereas HDACs remove the acetyl groups from the lysine residues during the deacetylation process [2]. The balance in this reversible mechanism by HATs and HDACs (i.e. acetylation and deacetylation) is vital for a normal gene transcription process to take place [3]. Increased acetylation of lysine is related with the transcription activation whereas, deacetylation results in transcription repression [4,5]. Especially, HDACs exhibit different mechanisms such as aberrant recruitment [6], mutations and altered level of gene expression [7,8], which play important roles in tumorigenesis.

The human HDAC family comprises eighteen HDAC enzymes, which are classified into four groups, class I, class II, class III and class IV, based on their homology and phylogeny with the yeast proteins [9,10]. The enzyme classes, class I (HDAC1, HDAC2, HDAC3 and HDAC8), class II (HDAC4–HDAC7, HDAC9–HDAC10) and class IV (HDAC11), are zinc dependent groups that share sequence and structural homology in their catalytic domains. On the other hand, the class III HDAC depends on the oxidized form of nicotinamide adenine dinucleotide (NAD+) for its activity [3,11–13]. A number of experiments have confirmed the over expression of the zinc dependent class I HDACs in different types of cancer [14,15], for instance, acute promyelocytic leukemia [5,16] and lung cancers [17]. Therefore, class I HDAC enzymes (HDAC1, HDAC2, HDAC3 and HDAC8) are considered among the most important targets for cancer therapy.

Several HDAC inhibitors (HDACIs) with different structural variants such as short-chain fatty acids, hydroxamic acids (HAs), cyclic tetrapeptides, cyclic peptides and benzamides have been reported [10,18,19], among which, a few of them are in clinical phases [20]. A number of studies indicate that the inhibitors from HA

* Corresponding author. Tel.: +61 3 9479 6768; fax: +61 3 9479 3060.
E-mail address: phoebe.chen@latrobe.edu.au (Y.-P.P. Chen).

1093-3263/$ – see front matter © 2013 Elsevier Inc. All rights reserved.
http://dx.doi.org/10.1016/j.jmgm.2013.05.002

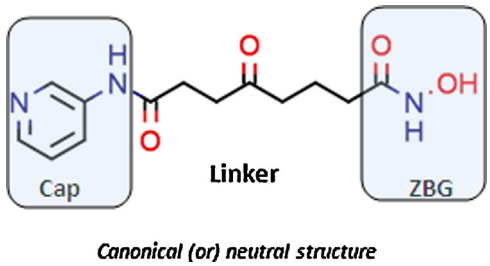

Fig. 1. General structural skeleton of HA inhibitors.

groups exhibit favorable characteristics against the class I HDAC enzymes [10,18,21]. Indeed, the common structural skeleton of HA inhibitors, which include a zinc binding group (ZBG), a linker and a cap, has been accepted as a more suitable template for designing HDAC inhibitors.

Fig. 1 presents the structural template of an HA inhibitor. The ZBG group in the HA chelates the catalytic zinc metal ion in the HDACs, whereas the capping group interacts with the surface regions of the HDACs and the linker connects the ZBG and the cap, by traversing through the 11 Å long active site channel in the HDACs [22,23]. The ZBG generally constitutes the HA group (R—C(=O)—NH—OH), where the oxygen atoms make a bidentate coordination with the catalytic zinc metal ion in order to preserve the 'His-Asp' charge transfer system [24] within the enzyme complex. The 'His-Asp' charge shuttle, which involves two histidine (His) residues, one tyrosine (Tyr) and two aspartate (ASP) residues, along with the other gate-keeping residues [23], plays a significant role in the deacetylation process of HDACs [24–26]. Especially, the two His residues exhibit an acid–base pair functionality for controlling the catalytic process of HDACs [27–29].

The significance of the protonation states of HA inhibitors have been reported in earlier studies [29–32], however, some results remain contradictory. For example, a previous DFT based study [30] reported that the deprotonated form of HA inhibitors (R—C(=O)—NH—O^-) show strong bidentate coordination with the zinc metal ion in the HDACs, while the neutral forms (R—CO—NH—OH) exhibit only monodentate coordination. In contrast, Tavakol, who studied a list of HA molecules along with their tautomers and transition states using DFT method, reported that the neutral or protonated form of HAs are the most stable structures [31]. Another recent study also found that the deprotonated form of SAHA (an HA inhibitor) is less stable than its neutral or protonated state [32]. This indicates that different protonation states of HA inhibitors can exhibit varied effects against the HDAC enzymes. However, systematic docking based studies on the impacts of different protonation states of HA inhibitors in the HDAC–inhibitor complexes are limited.

Different challenging issues such as, the stability of the tautomeric states, their synthetic feasibility and lack of relevant experimental details and molecular descriptors of these forms in the databases, limit the studies on the protonation states of inhibitors in the drug discovery processes. Nevertheless, with the rapid advancements in the enumeration capabilities of the cheminformatics programs and the state of the art hybrid quantum mechanics (QM) and molecular mechanics (MM) approaches, such limitations can be significantly reduced.

In this study, we explore the effects of different protonation states of HA inhibitors against the class I HDAC enzymes, using the hybrid quantum polarized ligand docking (QPLD) and the MM-generalized Born, surface area (MM-GBSA) [33,34] calculations. The neutral or canonical structures of the selected HA inhibitors, along with their protonated, deprotonated and classical tautomer states are considered. The impacts of different protonation states of the inhibitors on their binding modes, inter-molecular hydrogen bonds, molecular electrostatic potentials and physicochemical properties are studied.

2. Materials and methods

2.1. Homology modeling

The X-ray crystal structures of the human HDAC2 protein (PDB ID: 3MAX) [35] and human HDAC8 protein (PDB ID: 1T67) [27] were retrieved from the Protein Data Bank (PDB) [www.rcsb.org] [36] and used in this work. The structures of HDAC1 and HDAC3 enzymes were constructed using the homology modeling approach. The amino acid sequences of the human HDAC1 with 482 residues (Swissprot id: Q13547) and HDAC3 with 428 residues (Swissprot id: O15379) were downloaded from the SWISS-PROT protein sequence database [www.expasy.ch/sprot/]. A sequence similarity search performed using the BLOSUM62 substitution matrix in the BLAST program identified the human HDAC2 and HDAC8 structures as suitable template structures. The HDAC2 sequence exhibit 93% and 63% of identities against HDAC1 and HDAC3, respectively, whereas the HDAC8 sequence represent 43% identity against the HDAC1 and HDAC3 enzymes. As a result, the experimental structures of HDAC2 (PDB id: 3MAX) and HDAC8 (PDB id: 1T67) were used to construct the three dimensional structures of HDAC1 and HDAC3 enzymes in this study. During the modeling process, the active site zinc metal ion from the template structures was extracted so as to retain the actual penta-coordination of the zinc ion in the modeled structures.

The quality of the modeled structures were verified using the SAVES structure analysis program [http://nihserver.mbi.ucla.edu/SAVES/], which integrated five different tools: Procheck [37], WhatCheck [38], Errat [39], Verify 3D [40], and Prove [41] to evaluate the qualities of protein structures. The structures of all class I HDACs, HDAC1, HDAC2, HDAC3 and HDAC8, were initially refined by correcting the missing side chain atoms (given in supplementary Table 1), assigning the bond orders and adding polar hydrogen atoms to the receptors. The metal ions and the residue protonation states were assigned using the Epik module. Following the structural refinements, all the target structures were energy-minimized using the OPLS2001 force field [42]. The Prime module of the Schrodinger drug discovery package [43,44] was employed for the modeling and the structural refinement procedures.

Note that the X-ray crystal structure of HDAC3 has been reported very recently in 2012 (PDB ID: 4A69) [45], when this work was already in process. As a result, the modeled structure of HDAC 3 in this study was compared with the recent experimental structure by superimposing them and an RMSD value of only 0.34 Å was obtained for their active sites. The superimposed structure of HDAC3 model and the X-ray crystal structure is given in Fig. 2. As it can be seen in the figure, the modeled and the experimental structures of HDAC3 enzyme agree very well, with only small differences in the some of the terminal loop regions in the structure. The zinc coordination geometries of the class I HDACs are given in supplementary Table 2. Therefore, the current study is based on the modeled 3D structure of HDAC3.

2.2. Ligand preparation

The protonated and the deprotonated states of the selected HA inhibitors were generated using the Ligprep program [46] in the Schrodinger suite, which employs Hammett and Taft methods [47], along with the ionization and tautomerization tools, in order to rapidly generate reliable and chemically viable

Fig. 2. The superimposed structures of the modeled and the X-ray crystal structure (PDB: 4A69) of HDAC3. Spring green-4A69; blue-model. (For interpretation of the references to color in figure legend, the reader is referred to the web version of the article.)

structures [47–49]. In addition, the classical style HA tautomers (i.e. [R—C(=O)(—NH—OH) ↔ R—C(—OH)(=N—OH)]) were manually constructed using the Chemaxon [50] program. All the neutral, protonated (p), deprotonated (dp) and classical tautomer (ct) states of the HDACIs were generated and optimized using the OPLS2005 force field [42,51]. Therefore, a total of twenty two inhibitors were used in this study, whose 2D structures are given in Table 1.

2.3. Quantum-polarized ligand docking

Accurate docking calculations of the protonated forms of the inhibitors into the active sites of metalloproteins, especially those with transition metal ions such as HDACs, require more advanced QM level treatment [52–55]. In this study, we employed hybrid QM/MM-based quantum polarized ligand docking (QPLD) method, in order to dock the inhibitors into the active sites of class I HDAC enzymes. Within the QPLD framework, the ligand atoms are treated at the QM level, whereas the HDAC receptors (including the zinc ion) are described using the OPLS force field parameters. The inclusion of even few receptor atoms, such as the active site metal ion and residues, in the QM region can be computationally expensive. Moreover defining the boundary between the QM and MM atoms can also be an issue during the docking calculations and scoring [56]. However, the partial charges and the protonation states of the receptor molecules were carefully described using the Epik module of the Schrodinger suite, where the active site zinc ion was assigned with a +2 atomic charge. In addition, the histidine (HIS) residue coordinating with the zinc ion was given an epsilon protonation state, while the other two HIS residues in the second shell of the HDACs active sites were assigned with delta protonation. All the HDAC receptor structures in this work were energy minimized using the OPLS2001 force field before proceeding with the QPLD calculations.

A receptor grid box of size 15 Å × 15 Å × 15 Å was generated for all the four class I HDAC enzymes with zinc (Zn^{2+}) as the center of the box. This receptor grid was used to define the position and shape of the HDAC's active site for performing the docking experiments. Thus, the pre-energy minimized HA inhibitors were initially docked into the active sites of HDACs, which is well defined by the receptor grid. The initial docking calculations were carried out using the standard Glide SP (standard precision) docking protocol, in order to generate the preliminary ligand poses for the HDACs. Subsequently, the single point calculations of the ligand poses, using the density functional theory (DFT) based Becke–Lee–Yang–Parr (BLYP)/6-31G* model were performed to calculate the polarizable charges of the HA inhibitors in this study. DFT methods have been efficient in accurately calculating the properties of neutral and tautomeric states of different molecules [50,57,58]. New sets of charges those were obtained from the QM/MM approach were assigned for the inhibitors by electrostatic potential (ESP) fitting. Finally, the HA inhibitors assigned with new partial charges were further re-docked into the HDAC enzymes, in order to obtain the most energetically favorable ligand poses. A number of previous studies indicate that QPLD approach is useful for the accurate scoring of the ligand–protein complexes [52,59,60].

Table 1
Chemical structures of the HAs used in this study.

	Neutral structure (NT)	Protonated (p)	Deprotonated (dp)	Classical tautomer (ct)
TSA	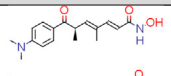	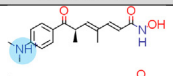	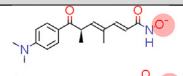	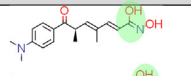
SK-7041	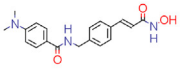	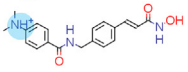	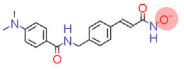	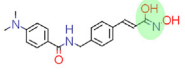
Laq-824	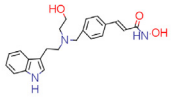	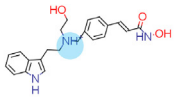	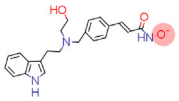	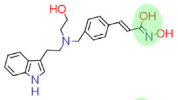
LBH-589	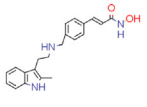	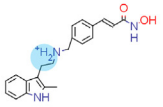	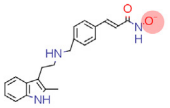	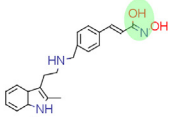
Oxamflatin	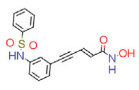		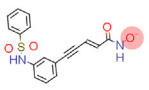	
Belinostat	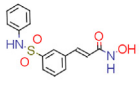		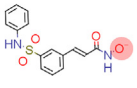	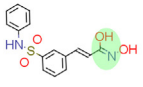

Table 2
Structure quality evaluation. Scores from the SAVES structure evaluation server.

	Ramachandran plot (%)				Verify-3D score (%)	ERRAT score (%)	*Z*-score
	Core region	Allowed regions	Generously allowed region	Disallowed region			
HDAC1	89.4	10.0	0.6	None	99.18	84.68	0.440
HDAC3	89.1	8.4	2.5	None	87.33	90.7	0.498

2.4. MM-GBSA calculation

Following the QPLD calculations, the MM-GBSA method was used to calculate the binding free energies, i.e. ΔG_b, of all the docked inhibitor–class I HDAC complexes. The ΔG_b for MM-GBSA approach can be written as [59],

$$\Delta G_b = \Delta E_{MM} + \Delta G_{GB} + \Delta G_{SA} - T\Delta S$$

where ΔE_{MM} is the minimum energy difference between the HA inhibitor–HDAC complexes and the sum of the energies of the unliganded HDACs and inhibitors. The ΔG_{GB} represents the electrostatic energy components calculated using the generalized-Born (GB) [61], which describes the polar contributions in the system. Whereas, the ΔG_{SA} describes the non-polar contribution to the solvation free energies of the complexes that is calculated using the solvent-accessible-surface-area approach [62,63]. The term $T\Delta S$ denotes the entropy that arise from the conformational changes in the system upon ligand binding into the receptor. The entropy can generally be decomposed into different contributions, such as translational, rotational and vibrational, which are estimated using normal-mode analysis. However, such a calculation requires large number of trajectories showing different conformations of the ligand–receptor complex, which is ultimately a memory intensive and computationally expensive process. In addition, insufficient numbers of sampling can lead to large uncertainties in the results [61,64,65]. Therefore, it is mostly preferred to avoid the entropy term, unless otherwise there are sufficiently large numbers and varieties of trajectories, and calculate the binding free energies with the ΔE_{MM} and ΔE_{solv} (i.e. $\Delta G_{GB} + \Delta G_{SA}$), which is known as the 'relative binding free energy'. The relative binding free energies with convincing accuracies can be achieved, even with a single post-docking snapshot and in limited computational cost, which is sufficient for computer aided drug design [61]. Therefore, the relative ΔG_b values of the inhibitor–HDAC complexes were calculated in the present study, in order to analyze the binding efficiencies of the different forms of HA inhibitors. All the free energy calculations in this study were carried out using the ligand and structure-based descriptor (LSBD) script [66] implemented in the Schrodinger drug discovery suite [66].

3. Results and discussion

3.1. Homology models of HDAC1 and HDAC3

The qualities of the modeled HDAC1 and HDAC3 enzymes are validated with respect to their peptide backbone conformations. The Ramachandran plots of the modeled HDAC1 and HDAC3 structures generated using the PROCHECK program are given in supplementary Fig. 1. The Ramachandran plot of the modeled HDAC1 enzyme displays 89.4% of the amino acid residues in the core region, 10% of residues within the allowed region and 0.6% at the generously allowed region. In the Ramachandran plot of HDAC3 model, 89.1% of residues are present in the core region, 8.4% in the allowed region and 2.5% in the generously allowed region. Moreover, there are no residues located in the disallowed regions of the plots in both the models. As a result, the modeled structures of HDAC1 and HDAC3 enzymes in this study present more appropriate stereo-chemical properties.

Table 2 compares the various scores of the HDAC1 and HDAC3 models that are obtained using the different structure evaluation programs (verify-3D, ERRAT and PROVE) in the SAVES server. The verify-3D scores of HDAC1 and HDAC3 models are 99.18% and 87.33%, respectively, which indicate that the modeled structures are perfectly compatible with their respective amino acid sequences. The non-bonded interaction scores in the ERRAT plot of the HDAC1 and HDAC3 structures also present high scores such as 84.68 (HDAC1) and 90.704 (HDAC3). Further, the atomic volumes of the modeled protein residues are evaluated for their consistencies with the equivalent residues in the PDB database and satisfactory *Z*-score mean values of 0.44 for HDAC1 and 0.49 for HDAC3 are obtained.

3.2. QPLD scoring of the inhibitor–HDAC complexes

The main objective of structure-based drug design is to identify the energetically favorable binding modes of ligands within the binding site of a target. Such information can provide valuable insights into the nature of the binding site and the key ligand–protein interactions that are responsible for molecular recognition [67,68]. The neutral and the protonation states (i.e. protonated, deprotonated and classical tautomers) of all HA inhibitors in this study are docked into the zinc binding sites of the class I HDAC enzymes, using the QPLD protocol (see methods section). The structure of the docked HDAC8–TSA (Trichostatin A, a hydroxamic acid based HDACI) complex that is obtained from the QPLD calculation is compared with the previously reported experimental HDAC8–TSA structure (PDB id: 1T64), by superimposing the former structure over the latter, as shown in Fig. 3. The hydroxamic acid group in TSA binds with the zinc metal ion in a bidentate mode,

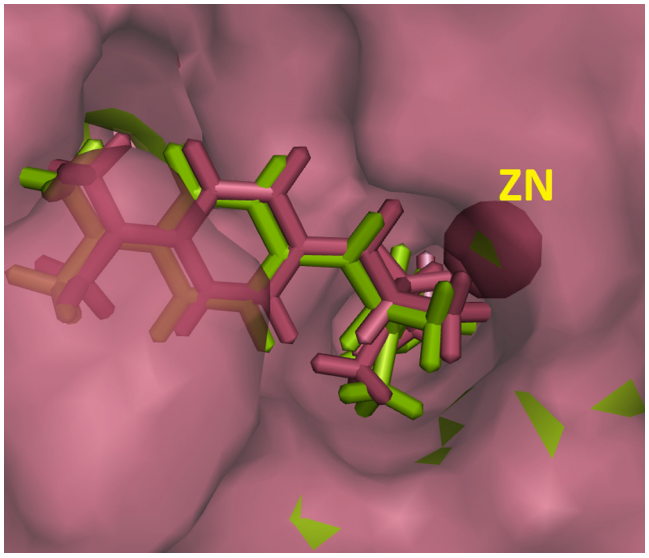

Fig. 3. Superimposed poses of the neutral TSA–HDAC8 structures from the QPLD model (pink) and the experiment (green). (For interpretation of the references to color in figure legend, the reader is referred to the web version of the article.)

the linear aliphatic linker of TSA occupies the 11 Å long active site channel and the aromatic capping group is placed in the surface of HDAC8. This indicates that QPLD protocol has reproduced the experimental binding modes of HDAC8–TSA complex very well, which can also be confirmed by their RMSD value < 0.5 Å.

Table 3 provides the QPLD scores (i.e. the docking scores) of all the inhibitor–class I HDAC complexes. The QPLD scores of all the protonated inhibitors against the class I HDACs (i.e. HDAC1, HDAC2, HDAC3 and HDAC8) are higher than their respective neutral and the other forms. The protonated form of TSA against HDAC1, HDAC2, HDAC3 and HDAC8 enzymes are 87.78 kcal mol^{-1}, 88.19 kcal mol^{-1}, 100.37 kcal mol^{-1} and 83.22 kcal mol^{-1}, respectively; those are higher than their corresponding neutral structures with QPLD scores of 86.67 kcal mol^{-1} (HDAC1), 86.61 kcal mol^{-1} (HDAC2), 85.77 kcal mol^{-1} (HDAC3) and 82.35 kcal mol^{-1} (HDAC8). Similar trends are seen in most of the protonated inhibitor–HDAC complexes, except oxamflatin and belinostat, whose protonated forms were not generated, as they did not pass the feasibility criteria in the Ligprep module. This indicates that the protonated forms of the HA inhibitors are able to display better complementarities against the class I HDACs than those of their respective neutral structures.

On the other hand, the deprotonated forms of the inhibitors exhibit lesser docking scores against the class I HDACs. For instance, the QPLD scores of the neutral oxamflatin–HDAC2 complex is 92.86 kcal mol^{-1}, while the score of the deprotonated oxamflatin–HDAC2 complex is only 74.55 kcal mol^{-1}. Such reduction in the QPLD scores of the deprotonated forms of the inhibitors in this study can be attributed to the weak non-bonded interactions between the deprotonated inhibitor and class I HDACs. Nevertheless, the classical tautomer forms of the inhibitors (as shown in Table 3) exhibit slightly higher scores than those of the deprotonated inhibitors, at the same time, lesser than their respective protonated and neutral structures.

The QPLD scores of the inhibitor–HDAC complexes presented in Table 3 mostly display a trend as, protonated > neutral > classical tautomer > deprotonated. For example, LAQ-824–HDAC3 depicts 120.05 kcal mol^{-1} (protonated) > 114.07 kcal mol^{-1} (neutral) > 106.31 kcal mol^{-1} (classical tautomer) > 87.49 kcal mol^{-1} (deprotonated). In an overall, the QPLD scores of the inhibitor–HDAC complexes are enhanced when the inhibitors are protonated, whereas the deprotonation, particularly at the zinc binding site of the inhibitors, reduce the docking scores. The intermolecular hydrogen bonds in the docked pose of HA inhibitor–HDAC complexes are also analyzed.

3.3. Intermolecular interactions of the inhibitor–HDAC complexes

Hydrogen bonds (H-bonds) play an active role in optimizing drug–protein affinities. In HDACs, the inter-molecular interactions

Table 3
Comparative QPLD scores and the MM-GBSA binding free energies of all the protonation states of HAs against class I HDAC enzymes. Energies of the neutral structures are highlighted in gray color.

Inhibitor/ID	I. QPLD based Docking Energy (values in negative k.cal mol^{-1})				II. MM-GBSA based Binding Free Energy (ΔG_b) (values in negative k.cal mol^{-1})			
	T1	T2	T3	T4	T1	T2	T3	T4
TSA (nt)	86.67	86.61	85.77	82.35	11.62$^{\$}$ (11.15)	11.12$^{\$}$ (10.91)	14.24$^{\$}$ (12.59)	22.82
p	87.78	88.19	100.37	83.22	13.43	14.39	21.99	20.12
ct	82.44	80.29	80.56	69.03	14.59	30.23	16.43	14.07
dp	66.13	67.69	63.51	65.08	87.72	93.72	86.80	82.08
SK-7041(nt)	91.54	89.71	88.84	90.24	17.37	17.03	17.42	27.90
p	103.31	103.11	104.02	91.90	19.50	23.93	19.49	29.52
ct	78.49	84.87	95.79	79.01	14.42	30.48	11.17	18.94
dp	71.78	71.26	66.23	71.98	96.90	94.92	80.84	70.72
LAQ-824 (nt)	102.38	102.06	114.07	103.74	15.08$^{\$}$ (10.98)	14.46$^{\$}$ (10.23)	18.59	26.55
p	107.75	104.89	120.05	99.07	15.73	15.84	22.31	29.21
ct	82.32	90.73	106.31	88.87	30.34	32.33	9.86	36.99
dp	82.15	81.55	87.49	87.59	93.39	95.99	94.44	90.08
LBH-589 (nt)	102.52	101.7	107.34	100.95	12.28	10.53	7.62	28.24
p	103.23	103.00	116.73	102.63	13.59	12.63	17.10	39.14
ct	90.64	96.73	95.24	96.00	26.77	10.45	5.83	3.60
dp	78.97	79.67	86.17	83.17	97.24	95.06	92.80	85.58
Oxamflatin (nt)	94.08	92.86	87.88	85.31	19.25	17.47	15.44	31.14
ct	85.58	88.86	84.98	77.33	21.20	23.32	3.87	17.71
dp	76.76	74.55	71.16	74.21	95.08	87.35	85.90	83.17
Belinostat (nt)	89.95	90.26	88.40	83.62	15.36	13.69	19.38	25.55
ct	77.00	77.04	93.29	69.81	1.77	25.06	32.12	22.80
dp	71.08	68.65	69.44	66.44	95.72	96.08	95.92	88.99

Abbreviations T1, T2, T3 and T4 represent the target structures, HDAC 1 (T1), HDAC 2 (T2), HDAC 3 (T3) and HDAC 8 (T4).
*nt: neutral; p: protonated; ct: classical tautomers; dp: deprotonated.
$Values given in parentheses are the experimental binding free energies from the online database at www.bindingdb.org.

adapted by the zinc binding group (ZBG) of the inhibitors participate in the Histidine-Aspartate (His-Asp) charge relay system, which is important for the functionalities of class I HDACs. The changes in protonation states of the inhibitors significantly affected the inter-molecular H-bonds networks within the inhibitor–HDAC complexes. The list of amino acid residues in the HDACs that are involved in the inter-molecular H-bonds is given in the supplementary Table 3.

The neutral forms of the inhibitors make all fingerprint H-bonds that are highly conserved to class I HDACs. The neutral forms of inhibitors in this study makes bidentate coordination (of distance ~2.0 Å) with the catalytic zinc metal ion, which further interacts with three metal coordinating residues (1 HIS and 2 ASP) in class I HDACs. In addition, the zinc binding group (ZBG) in the neutral inhibitors accepts H-bonds from a TYR residue (303 in HDAC1; 304 in HDAC2; 297 in HDAC3; 306 in HDAC8) via a [(TYR)O—H···O=C(ZBG)] bond and donates H-bonds to 2 HIS residues (140, 141 in HDAC1; 141, 142 in HDAC2; 134,135 in HDAC3;142,143 in HDAC8) via [(ZBG)N—H···N(HIS1)] and [(ZBG)N—H···N(HIS2)] bonds. Such inter-molecular interactions are known as fingerprint interactions in the inhibitor–HDAC complexes that are significant for stabilizing the 'His-Asp' charge relay processes in class I HDACs. The zinc coordination distances in all the complexes are provided in Table 4, which excellently agree with the experimental values from the literature [30,69]. Fig. 4a presents the interactions between the neutral SK-7041 and the active site residues of HDAC8 enzyme. As it can be seen in the figure, the neutral ligand exhibits all the above-mentioned chemical bonds against the target, including bidentate coordination with the zinc (with both Zn—O distances at ~2.0 Å) and H-bonds with TYR 306, HIS 142 and HIS 143.

In the case of the protonated HA inhibitors, they display inter-molecular bonding architectures that are similar to those of the neutral forms, along with a few additional H-bonds against the target. For instance, Fig. 4b presents the interactions between the protonated SK-7041 and the HDAC8 enzyme. The bonding characteristics of the protonated SK-7041–HDAC8 complex (Fig. 4b) are similar to those found in the neutral SK-7041–HDAC8 complex (Fig. 4a). This suggests that protonating the HA inhibitors in their cap and linker regions does not affect the inter-molecular interactions within the inhibitor–class I HDAC complexes. Further experiments in the direction can be encouraging.

The classical tautomer and the deprotonated inhibitors display certain similarities in the fingerprint H-bonds such as TYR–ZBG interactions (refer to supplementary Table 3 for residues) in all the complexes. However, the interactions between the ligand and the class I HDACs are affected in response to the removal of a proton from the ZBG of the inhibitors (i.e. to form classical tautomers and deprotonated forms). When the O(H) group in the ZBGs is deprotonated (dp), this oxygen atom becomes more electronegative (i.e. O(H) becomes O^-) and binds very strongly with the zinc metal ion in the HDACs. This in turn, weakens the bond between the other oxygen atom, O(=C), and the zinc ion. For instance, Zn—O(H) and Zn—O(=C) distances in the neutral SK-7041–HDAC8 complex are 2.12 Å and 2.00 Å, respectively (as provided in Table 4). However, in the deprotonated form of SK-7041–HDAC8 complex, the Zn—O^- distance shrinks to 1.86 Å and the Zn—O(=C) length increases to 2.37 Å, leading to bidentate coordination with the zinc. This is in correlation with the previous QM/MM simulation that reported bidentate coordination between the deprotonated SAHA and HDAC8 enzyme [32].

For example, Fig. 4c shows the interaction between the deprotonated SK-7041 and HDAC8 enzyme. Although, the deprotonated SK-7041 maintains a bidentate coordination with the catalytic zinc metal in HDAC8, an important H-bond between the inhibitor and the active site HIS residue [(HIS)N···H—N(ZBG)] in the HDAC is found to be absent, which results in the disruption of the His-Asp charge transfer machinery within the HDAC enzymes. That is, a bond between HIS142 and the ZBG is not present in the deprotonated SK-7041 and HDAC8 complex. This indicates that, despite the fact that the deprotonation of ZBG in the inhibitors does not significantly affect its bidentate coordination with the active site zinc metal ion, it tends to break the key interactions involved in the His-Asp charge relay system of HDACs.

Conversely, the classical tautomer forms of inhibitors do not present bidentate coordination with the zinc metal ion in HDACs, but only a monodentate bonding. This is because, the hydrogen atom from the nitrogen is transferred to the carbonyl oxygen, thereby leaving a second hydroxyl group in the ZBGs of the classical tautomers (HO—N=C—OH) against the neutral form

Table 4
Zn—O (ZBG) distances from all the HA–HDAC complexes.

Name	HDAC 1		HDAC 2		HDAC 3		HDAC 8	
	ZN—O[H]	ZN—O[=C]	ZN—O[H]	ZN—O[=C]	ZN—O[H]	ZN—O[=C]	ZN—O[H]	ZN—O[=C]
TSA (nt)	2.12	2.01	2.12	2.00	2.06	1.99	2.09	2.04
p	2.12	2.00	2.12	2.01	2.12	2.00	2.09	2.04
ct	1.84	4.25	1.92	4.33	1.90	3.97	2.07	4.02
dp	1.86	2.45	1.86	2.48	1.86	2.62	2.04	2.21
SK-7041 (nt)	2.12	2.00	2.12	2.00	2.10	2.03	2.09	2.01
p	2.12	2.01	2.12	2.01	2.11	2.03	2.08	2.07
ct	1.95	4.05	2.07	4.36	1.90	3.91	2.04	4.32
dp	1.86	2.54	1.86	2.57	1.86	2.47	1.86	2.37
LAQ-824 (nt)	2.12	2.01	2.12	2.01	2.10	2.00	2.10	2.02
p	2.12	2.01	2.12	2.02	2.10	2.01	2.10	2.02
ct	2.04	3.16	1.94	4.27	1.93	3.89	2.1	3.85
dp	1.86	2.52	1.86	2.49	1.86	2.43	1.86	2.36
LBH-589 (nt)	2.13	2.01	2.13	2.01	2.10	2.00	2.09	2.03
p	2.12	2.00	2.13	2.01	2.10	2.00	2.10	2.02
ct	1.85	4.25	1.90	4.28	1.89	3.17	2.10	4.07
dp	1.86	2.58	1.86	2.49	1.86	2.47	1.87	2.43
Oxamflatin (nt)	2.12	2.00	2.12	2.00	2.11	2.00	2.08	2.02
ct	1.95	3.50	2.12	4.29	1.98	3.18	2.08	3.94
dp	1.86	2.58	1.85	2.55	1.86	2.61	1.86	2.43
Belinostat (nt)	2.12	2.02	2.12	2.00	2.11	2.00	2.09	2.03
ct	1.97	3.39	2.24	4.22	1.86	3.94	2.09	3.15
dp	1.86	2.50	1.86	2.52	1.86	2.50	1.86	2.42

nt: neutral; p: protonated; ct: classical tautomers; dp: deprotonated.

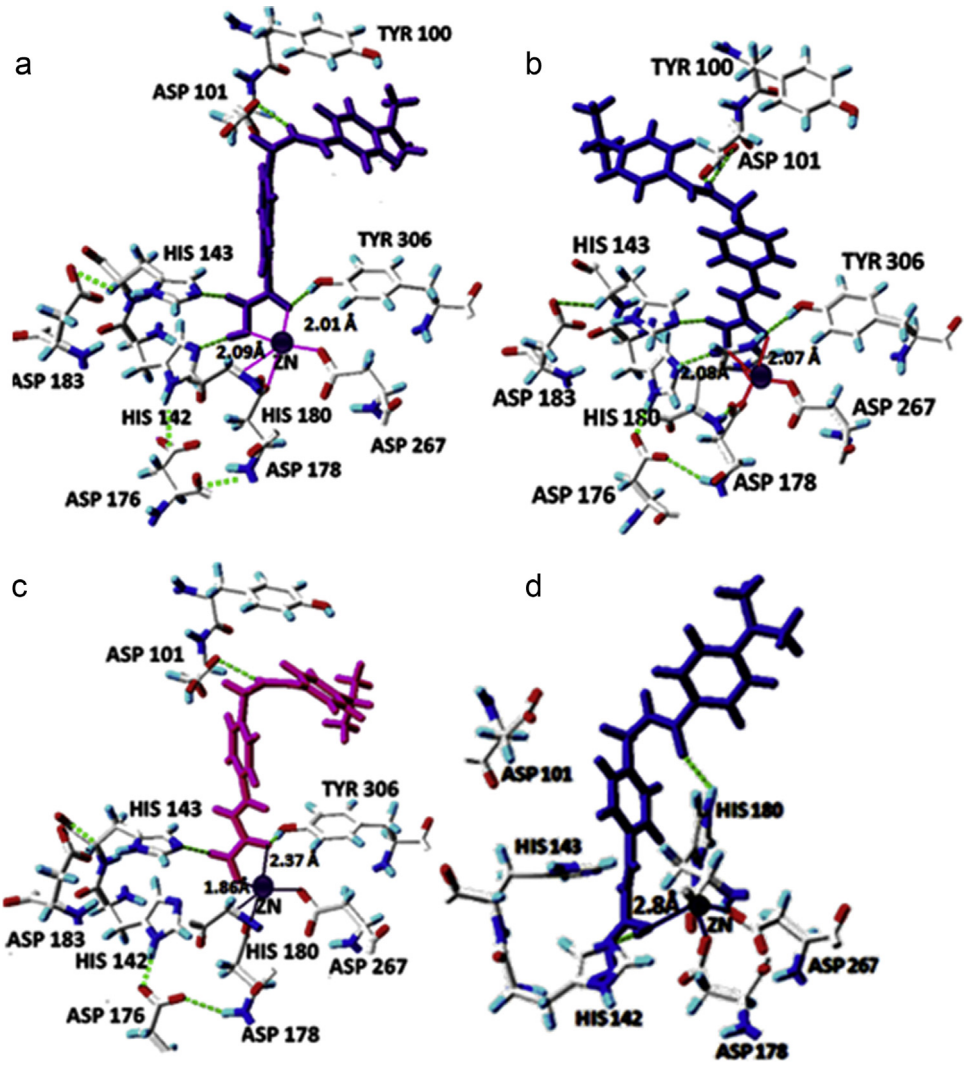

Fig. 4. Major inter-molecular bonds, including H-bonds (dotted lines) and zinc coordination (solid lines), within the (a) neutral, (b) protonated, (c) deprotonated and (d) classical tautomer forms of SK-7041 and the experimental HDAC8 structure.

(HO—N(H)—C=O). This second hydroxyl group (i.e. (C—)OH) in the classical tautomers competes with the native hydroxyl group (HO(—N)) to establish the hydrogen bonds with the surrounding active site residues, mostly HIS and GLY (refer to supplementary Table 3 for corresponding residue numbers). As a consequence, one of the hydroxyl group (i.e. (C)—OH) makes inter-molecular H-bonds and the other hydroxyl group (HO(—N)) establishes a strong zinc binding (<2.0 Å). For instance, Fig. 4d presents the H-bond interactions between the classical tautomers SK-7041–HDAC8 complexes, where both the hydroxyl group in ZBG makes an H-bond with the HIS142. Therefore, one of the Zn—O bond is approximately 4.32 Å, while the other Zn—O bond length is 2.04 Å. Similar trends are observed in most of the classical tautomers–HDAC complexes (refer to Table 4). The results, therefore, suggest that the removal of a hydrogen atom from the zinc binding group of the inhibitor disturbs the inter-molecular interactions between the inhibitor–HDAC complexes.

3.4. Molecular electrostatic potential (MEP) and physico-chemical properties

Information on physico-chemical properties such as solubility, hydrophobicity and electrostatic features remain the essence of any protonation-based studies. However, the accurate prediction of such inherent molecular properties remains a challenge due to the lack of enough experimental details that can assist in computational predictions. Herein, with the available resources and more reliable algorithms, we have extended our investigations toward a number of structural parameters including molecular electrostatic potentials (MEPs), log S and log P of all the structures. The MEPs of the protonation states of HAs are given in supplementary Table 3 and the molecular descriptors are given in supplementary Table 4. Log S and log P values (supplementary Table 4) of all the structures are in a similar range, indicating that the solubility and hydrophobicity factors of the protonated and neutral forms are similar. However, the classical tautomers are predicted to possess higher solubility and octanol–water partition co-efficient than the other forms. Further, the MEPs of the inhibitors (supplementary Table 3) display charge re-distributions within the inhibitors in response to their tautomeric nature. The MEPs of the neutral and the protonated forms are close to each other, while those of deprotonated and classical tautomers are different indicating their possible effects to the electrostatic interactions within the complexes. This interpretation is further analyzed using the MM-GBSA based binding free energy calculations.

3.5. MM-GBSA calculation of the inhibitor–HDAC complexes

The binding free energies of all the inhibitor–HDAC complexes that are calculated using the MM-GBSA approach, along with the available experimental values of TSA and LAQ-824 are given in Table 3. The experimental binding free energy of TSA and LAQ-824 are obtained from the previously reported inhibition constant (IC_{50}) values (taken from the bindingdb database available at www.bindingdb.org), using the equation [70],

$$\Delta G_{exp} = RT \ln(IC_{50}).$$

Here R represents the universal gas constant and T is the temperature in Kelvin. The calculated binding free energies of TSA and LAQ-824 present a reasonable agreement (of <5 kcal mol^{-1}) with the experimental values, which confirms the applicability of the MM-GBSA approach for the systems in the present study. However, the MM-GBSA calculations exhibit a completely different ranking of the inhibitors against the QPLD calculations. Indeed the deprotonated inhibitors in the MM-GBSA rescoring exhibit unrealistic values against the class I HDACs. As shown in the MM-GBSA results in Table 3, the ΔG_b values of the deprotonated ligands span between ~70 kcal mol^{-1} and 98 kcal mol^{-1}, which are up to 54 times larger than the other forms of the inhibitors in this study. For instance, the ΔG_b values of the different forms of SK-7041 against HDAC1 are 19.50 kcal mol^{-1} (protonated) > 17.37 kcal mol^{-1} (neutral) > 14.42 kcal mol^{-1} (classical tautomer). However, the free energy value for the deprtonated SK-7041–HDAC1 complex is 96.90 kcal mol^{-1}. This indicates that the theoretical model in this study, despite being able to calculate accurately predict the neutral and protonated inhibitors, has not been able to estimate the binding free energies of the deprotonated inhibitors to a satisfactory level of accuracy.

The different energetic terms of the HA inhibitors, such as the molecular mechanics contributions ($\Delta G_{(coulomb)}$, $\Delta G_{(covalent)}$, $\Delta G_{(vdw)}$) and the non-polar ($\Delta G_{(SA)}$) and the polar ($\Delta G_{(GB)}$) energy terms, were decomposed from the MM-GBSA calculations, which are given in the supplementary Table 5. The polar electrostatic solvation energy computed by GB ($\Delta G_{(GB)}$) and the coulombic energy terms in the deprotonated ligands, estimated by the MM-GBSA approach, consistently vary about hundreds of kcal mol^{-1} with respect to the neutral or protonated forms. The removal of the hydrogen atom from the hydroxyl group leaves a strongly active zinc binding groups (ZBGs) in the deprotonated HA inhibitors, which in turn alters the electrostatic interactions in the inhibitor–HDAC complexes. This is in agreement with the previous studies, which indicated that the effects of atomic charges of the ligand may impact the electrostatic and polar terms in binding free energies of the system [33,71–74]. The non-polar energy term ($\Delta G_{(SA)}$) is the least affected component in the binding free energy because of the protonation states of the HA inhibitor, whereas the van der Waals and covalent terms exhibit only smaller magnitude of changes in the MM-GBSA calculations of the inhibitor–HDAC complexes given in the supplementary Table 5.

Thus our study provides a qualitative description of the changes in the binding free energies of the complexes relative to the deprotonated forms of HA inhibitors against the other forms, despite the MM-GBSA approach breaking down in the former case. More accurate estimation of the absolute binding energies of the different protonation states of HA inhibitors may require the inclusion of entropy terms to the calculations, which was not within the reach of the present study. The estimation of the entropy change in the system requires extensive minimization of the trajectory conformations of the ligand, protein and the complex, which is followed by the normal mode analysis calculations. Such a procedure remains extremely memory intense and computationally expensive. Moreover, sufficiently large numbers and varieties of conformational sampling of the ligand–protein complexes are required in order to make acceptable entropy calculations, without which the estimation can lead to higher uncertainties.

The conformational sampling of the ligand–protein complexes are usually obtained from long molecular dynamics (MD) trajectories. Two different types of MD trajectory approximations are generally employed to calculate the entropy, such as the 'single-trajectory' approach and the 'three-trajectory' approach. In the former approach, a single state trajectory for the ligand–protein complex is used for the entropy calculation, whereas in the latter, three different trajectories for the ligand, protein and the ligand–protein complex are employed for the entropy calculations. The translational, rotational and vibrational contributions from the conformational trajectories are computed using the normal mode analysis, in order to calculate the entropy changes in the system. However, the lengths of the MD simulations and the number of trajectories required for accurate calculation of the absolute binding free energies are not always obvious and can be very much system specific. In addition, the charge method employed in the MD simulation are known to have profound impacts in the free energy calculations, i.e. the conformations of a complex sampled by MD using one type of force field may not be valid for any other force field. Such inconsistencies in the force field methods can again lead to large differences in the $\Delta G_{(electrostic)}$ and $\Delta G_{(GB)}$ composing the MM-GBSA method.

Infact, binding free energy calculations performed with entropy term can also lead to uncertain results. For instance, Oehme et al. reported that even with the inclusion of the entropy contributions by means of very expensive MD simulations, the calculated absolute binding free energies of some of the charged ligand–HIV protease systems were erroneous with unrealistic values [71]. Recently, calculations of the binding free energies from the state of the art hybrid QM/MM MD trajectories have become attractive, where the ligand and the selected receptor molecules are given pure QM treatment during MD simulations. The advantage of such approach is that incompatibilities of force field parameters for the protonated ligands can be overcome, as the charges of the molecules under QM framework are calculated on the fly. Yet, the state of the art approach comes with a hefty computational cost than those of the classical MD/MM-GBSA approaches.

On the other hand, MM-GBSA calculations excluding the entropy terms on a single docking pose of the complexes has resulted in higher correlation between the calculated and experimental binding free energies (Du 2011, Hou 2011b, Lyne 2006 in 9). This has also been achieved in this study for the neutral TSA–HDAC and LAQ-824–HDAC complexes. Moreover, leaving behind the break down in the free energy calculations of the deprotonated inhibitors, the MM-GBSA approach in this study has been able to satisfactorily calculate the values and rank the protonated and neutral HA inhibitors.

The overall motive of this study was to study the impacts of different protonation states of the hydroxamic acid inhibitors against the class I HDACs using the combined QPLD and MM-GBSA approaches. Although such goal has not be completely achieved, our results do indicate that the additionally protonated forms of HA inhibitors exhibit favorable interactions as the neutral molecules. Further investigations using the large scale MD simulations of the different forms of HA inhibitors and HDAC complexes have been initiated, whose results may be useful to better understand their interactions in future. The present study also describes the weaknesses in the present MM-GBSA approach toward the calculations of binding free energies of the deprotonated forms of HA inhibitors. Apart from several technical issues in the inclusion of tautomers in the computational drug design, such as the stability of tautomers

states, synthetic feasibility and lack of experimental details, even the well established approaches are not able to tackle the computations of charged state of inhibitors. Therefore, improvement of the available solvent models and force field parameters to suit the different states of ligand–protein complexes, besides the development of new models become inevitable in the modern computational drug discovery efforts.

4. Conclusion

The binding modes of the inhibitors and their inter-molecular interactions with class I HDACs, in response to the different protonation states of the inhibitors, such as protonated, deprotonated and classical tautomers, have been explored. The hybrid QPLD and MM-GBSA approaches have been employed. Our results indicate that the different protonation forms of inhibitors show significant similarities and differences in their interactions with the class I HDACs. The QPLD results show that the protonated states of inhibitors display higher scores in all the class I HDACs, while the deprotonated inhibitors present lower scores. The hydrogen bond analysis on the binding modes of HA–HDAC complexes predicted by the QPLD calculations found that the protonated inhibitors present more favorable binding modes and interactions with the class I HDACs. However, the deprotonated and the classical tautomers tend to disturb the interactions and the 'Histidine-Aspartate' charge relay residues. The molecular electrostatic potentials and the other physico-chemical descriptors also supported the results.

In general, the MM-GBSA approach in this study predicted more accurate binding energies for the neutral and the protonated inhibitors, which were in satisfactory agreement with the experiments. While the binding free energies of the protonated inhibitors were reasonably higher (more negative) than the neutral forms, in correlation with the QPLD calculations, the free energies of the deprotonated forms were found to be erroneous with unrealistically large values. Especially, the polar electrostatic solvation energy computed by GB ($\Delta G_{(GB)}$) and the coulomb energy terms in the deprotonated ligands, estimated by the MM-GBSA approach, were found to consistently vary about hundreds of kcal mol^{-1} with respect to the neutral or protonated forms. This indicates that the present MM-GBSA model has not been able to accurately estimate the free energies of the deprotonated inhibitors. Inclusion of the entropy terms to calculate the total absolute binding free energies could improve the results, however, such calculations impose hefty computational costs. It is important to note that a number of studies indicate that MM-GBSA with the entropy terms does not change the binding free energy very much and sometimes the values are unrealistic, as well. Therefore, despite the MM-GBSA method been demonstrated as an efficient tool in the computational drug design, the approach is still not sufficient for the binding free energy calculations of charge intense systems, such as the deprotonated inhibitors in this study. Therefore much higher levels of simulations, QM/MM molecular dynamics for instance, can be useful for the investigations on the deprotonated inhibitors, which will be our next focus of study.

In conclusion, apart from a number of technical and feasibility issues facing the studies of tautomers in computer aided drug design, the well established approaches, such as the MM-GBSA, are also not able to efficiently handle the computations of charged states of inhibitors. Therefore, improvements of the available models and force fields and the development of new models to suit wide rage of systems are essential to enjoy the full advantages of the computer-assisted drug discovery, that is, valuable science at affordable computing costs and time.

Acknowledgements

KS acknowledges the Faculty of Science, Technology and Engineering La Trobe University – Postgraduate Research Scholarships (FSTE-LTUPRS) and the PhD top-up scholarships from Victorian Life Sciences Computation Initiative (VLSCI). Authors would like to thank the reviewers for their very constructive suggestions, which have been useful for the revision of this paper. VLSCI and Victorian Partnership for Advanced Computing (VPAC) are acknowledged for the Supercomputing time.

Appendix A. Supplementary data

Supplementary data associated with this article can be found, in the online version, at http://dx.doi.org/10.1016/j.jmgm.2013.05.002.

References

[1] O. Martínez-Iglesias, L. Ruiz-Llorente, R. Sánchez-Martínez, L. García, A. Zambrano, A. Aranda, Histone deacetylase inhibitors: mechanism of action and therapeutic use in cancer, Clinical and Translational Oncology 10 (2008) 395–398.
[2] M.-H Kuo, C.D. Allis, Roles of histone acetyltransferases and deacetylases in gene regulation, BioEssays 20 (1998) 615–626.
[3] M. Grunstein, Histone acetylation in chromatin structure and transcription, Nature 389 (1997) 349–352.
[4] C.M. Grozinger, S.L. Schreiber, Deacetylase enzymes: biological functions and the use of small-molecule inhibitors, Chemistry and Biology 9 (2002) 3–16.
[5] D. Mottet, V. Castronovo, Histone deacetylases: target enzymes for cancer therapy, Clinical and Experimental Metastasis 25 (2008) 183–189.
[6] H. Matsushita, P.P. Scaglioni, M. Bhaumik, E.M. Rego, L.F. Cai, S.M. Majid, H. Miyachi, A. Kakizuka, W.H. Miller, P.P. Pandolfi, In vivo analysis of the role of aberrant histone deacetylase recruitment and RARα blockade in the pathogenesis of acute promyelocytic leukemia, Journal of Experimental Medicine 203 (2006) 821–828.
[7] P. Gallinari, S.D. Marco, P. Jones, M. Pallaoro, C. Steinkuhler, HDACs, histone deacetylation and gene transcription: from molecular biology to cancer therapeutics, Cell Research 17 (2007) 195–211.
[8] A. Hagelkruys, A. Sawicka, M. Rennmayr, C. Seiser, The biology of HDAC in cancer: the nuclear and epigenetic components, in: T.-P. Yao, E. Seto (Eds.), Histone Deacetylases: The Biology and Clinical Implication, 206, Springer, Berlin Heidelberg, 2011, pp. 13–37.
[9] S.C. Hodawadekar, R. Marmorstein, Chemistry of acetyl transfer by histone modifying enzymes: structure, mechanism and implications for effector design, Oncogene 26 (2007) 5528–5540.
[10] M. Dokmanovic, P.A. Marks, Prospects: histone deacetylase inhibitors, Journal of Cellular Biochemistry 96 (2005) 293–304.
[11] J.E. Bradner, N. West, M.L. Grachan, E.F. Greenberg, S.J. Haggarty, T. Warnow, R. Mazitschek, Chemical phylogenetics of histone deacetylases, Nature Chemical Biology 6 (2010) 238–243.
[12] S.V.W. Weerasinghe, G. Estiu, O. Wiest, M.K.H. Pflum, Residues in the 11 Ã channel of histone deacetylase 1 promote catalytic activity: implications for designing isoform-selective histone deacetylase inhibitors, Journal of Medicinal Chemistry 51 (2008) 5542–5551.
[13] H. Tang, X.S. Wang, X.-P. Huang, B.L. Roth, K.V. Butler, A.P. Kozikowski, M. Jung, A. Tropsha, Novel inhibitors of human histone deacetylase (HDAC) identified by QSAR modeling of known inhibitors, virtual screening, and experimental validation, Journal of Chemical Information and Modeling 49 (2009) 461–476.
[14] B.H. Huang, M. Laban, C.H.W. Leung, L. Lee, C.K. Lee, M. Salto-Tellez, G.C. Raju, S.C. Hooi, Inhibition of histone deacetylase 2 increases apoptosis and p21Cip1//WAF1 expression, independent of histone deacetylase 1, Cell Death and Differentiation 12 (2005) 395–404.
[15] P. Zhu, E. Martin, J. Mengwasser, P. Schlag, K.-P. Janssen, M. Göttlicher, Induction of HDAC2 expression upon loss of APC in colorectal tumorigenesis, Cancer Cell 5 (2004) 455–463.
[16] R.J. Lin, L. Nagy, S. Inoue, W. Shao, W.H. Miller, R.M. Evans, Role of the histone deacetylase complex in acute promyelocytic leukaemia, Nature 391 (1998) 811–814.
[17] J.W. Neal, L.V. Sequist, Complex role of histone deacetylase inhibitors in the treatment of non-small-cell lung cancer, Journal of Clinical Oncology 30 (2012) 2280–2282.
[18] P.A. Marks, V.M. Richon, T. Miller, W.K. Kelly, F.V.W. George, K. George, Histone Deacetylase Inhibitors. Advances in Cancer Research, 91, Academic Press, 2004, pp. 137–168.
[19] C.A. Lyssiotis, L.L. Lairson, A.E. Boitano, H. Wurdak, S. Zhu, P.G. Schultz, Chemical control of stem cell fate and developmental potential, Angewandte Chemie International Edition 50 (2011) 200–242.
[20] K. Garber, HDAC inhibitors overcome first hurdle, Nature Biotechnology 25 (2007) 17–19.

[21] A. Mai, S. Massa, D. Rotili, I. Cerbara, S. Valente, R. Pezzi, S. Simeoni, R. Ragno, Histone deacetylation in epigenetics: an attractive target for anticancer therapy, Medicinal Research Reviews 25 (2005) 261–309.
[22] K.V. Balakin, Y.A. Ivanenkov, A.S. Kiselyov, S.E. Tkachenko, Histone deacetylase inhibitors in cancer therapy: latest developments, trends and medicinal chemistry perspective, Anti-Cancer Agents in Medicinal Chemistry 7 (2007) 576–592.
[23] S. Kalyaanamoorthy, Y.-P.P. Chen, Exploring inhibitor release pathways in histone deacetylases using random acceleration molecular dynamics simulations, Journal of Chemical Information and Modeling 52 (2012) 589–603.
[24] M.S. Finnin, J.R. Donigian, A. Cohen, V.M. Richon, R.A. Rifkind, P.A. Marks, R. Breslow, N.P. Pavletich, Structures of a histone deacetylase homologue bound to the TSA and SAHA inhibitors, Nature 401 (1999) 188–193.
[25] M. Schapira, Structural biology of human metal-dependent histone deacetylases, in: T.-P. Yao, E. Seto (Eds.), Histone Deacetylases: The Biology and Clinical Implication, 206, Springer, Berlin Heidelberg, 2011, pp. 225–240.
[26] A.J.M. de Ruijter, A.H. van Gennip, H.N. Caron, S. Kemp, A.B.P. van Kuilenburg, Histone deacetylases (HDACs): characterization of the classical HDAC family, Biochemical Journal 370 (2003) 737–749.
[27] J.R. Somoza, R.J. Skene, B.A. Katz, C. Mol, J.D. Ho, A.J. Jennings, C. Luong, A. Arvai, J.J. Buggy, E. Chi, J. Tang, B.-C. Sang, E. Verner, R. Wynands, E.M. Leahy, D.R. Dougan, G. Snell, M. Navre, M.W. Knuth, R.V. Swanson, D.E. McRee, L.W. Tari, Structural snapshots of human HDAC8 provide insights into the class I histone deacetylases, Structure (London, England: 1993) 12 (2004) 1325–1334.
[28] S.L. Gantt, C.G. Joseph, C.A. Fierke, Activation and inhibition of histone deacetylase 8 by monovalent cations, Journal of Biological Chemistry 285 (2010) 6036–6043.
[29] R. Wu, S. Wang, N. Zhou, Z. Cao, Y. Zhang, A proton-shuttle reaction mechanism for histone deacetylase 8 and the catalytic role of metal ions, Journal of the American Chemical Society 132 (2010) 9471–9479.
[30] D. Wang, P. Helquist, O. Wiest, Zinc binding in HDAC inhibitors: a DFT study, Journal of Organic Chemistry 72 (2007) 5446–5449.
[31] H. Tavakol, Computational study of simple and water-assisted tautomerism of hydroxamic acids, Journal of Molecular Structure: THEOCHEM 916 (2009) 172–179.
[32] R. Wu, Z. Lu, Z. Cao, Y. Zhang, Zinc chelation with hydroxamate in histone deacetylases modulated by water access to the linker binding channel, Journal of the American Chemical Society 133 (2011) 6110–6113.
[33] B. Kuhn, P.A. Kollman, Binding of a diverse set of ligands to avidin and streptavidin: an accurate quantitative prediction of their relative affinities by a combination of molecular mechanics and continuum solvent models, Journal of Medicinal Chemistry 43 (2000) 3786–3791.
[34] J. Srinivasan, T.E. Cheatham, P. Cieplak, P.A. Kollman, D.A. Case, Continuum solvent studies of the stability of DNA, RNA, and phosphoramidate DNA helices, Journal of the American Chemical Society 120 (1998) 9401–9409.
[35] J.C. Bressi, A.J. Jennings, R. Skene, Y. Wu, R. Melkus, R.D. Jong, S. O'Connell, C.E. Grimshaw, M. Navre, A.R. Gangloff, Exploration of the HDAC2 foot pocket: synthesis and SAR of substituted N-(2-aminophenyl)benzamides, Bioorganic and Medicinal Chemistry Letters 20 (2010) 3142–3145.
[36] H.M. Berman, J. Westbrook, Z. Feng, G. Gilliland, T.N. Bhat, H. Weissig, I.N. Shindyalov, P.E. Bourne, The Protein Data Bank, Nucleic Acids Research 28 (2000) 235–242.
[37] R.A. Laskowski, M.W. Macarthur, D.S. Moss, J.M. Thornton, PROCHECK: a program to check the stereochemical quality of protein structures, Journal of Applied Crystallography 26 (1993) 283–291.
[38] R.W.W. Hooft, G. Vriend, C. Sander, E.E. Abola, Errors in protein structures, Nature 381 (1996) 272.
[39] C. Colovos, T.O. Yeates, Verification of protein structures: patterns of nonbonded atomic interactions, Protein Science 2 (1993) 1511–1519.
[40] R. Luthy, J.U. Bowie, D. Eisenberg, Assessment of protein models with three-dimensional profiles, Nature 356 (1992) 83–85.
[41] J. Pontius, J. Richelle, S.J. Wodak, Deviations from standard atomic volumes as a quality measure for protein crystal structures, Journal of Molecular Biology 264 (1996) 121–136.
[42] G.A. Kaminski, R.A. Friesner, J. Tirado-Rives, W.L. Jorgensen, Evaluation and reparametrization of the OPLS-AA force field for proteins via comparison with accurate quantum chemical calculations on peptides†, Journal of Physical Chemistry B 105 (2001) 6474–6487.
[43] M.P. Jacobson, R.A. Friesner, Z. Xiang, B. Honig, On the role of the crystal environment in determining protein side-chain conformations, Journal of Molecular Biology 320 (2002) 597–608.
[44] M.P. Jacobson, D.L. Pincus, C.S. Rapp, T.J.F. Day, B. Honig, D.E. Shaw, R.A. Friesner, A hierarchical approach to all-atom protein loop prediction, Proteins: Structure, Function, and Bioinformatics 55 (2004) 351–367.
[45] P.J. Watson, L. Fairall, G.M. Santos, J.W.R. Schwabe, Structure of HDAC3 bound to co-repressor and inositol tetraphosphate, Nature (2012), Advance Online Publication.
[46] LigPrep, version 2.5, Schrödinger, LLC; New York, NY, 2011.
[47] J. Shelley, A. Cholleti, L. Frye, J. Greenwood, M. Timlin, M. Uchimaya, Epik: a software program for p*K*a prediction and protonation state generation for drug-like molecules, Journal of Computer-Aided Molecular Design 21 (2007) 681–691.
[48] M.-S. Park, C. Gao, H.A. Stern, Estimating binding affinities by docking/scoring methods using variable protonation states, Proteins: Structure, Function, and Bioinformatics 79 (2011) 304–314.
[49] J. Greenwood, D. Calkins, A. Sullivan, J. Shelley, Towards the comprehensive, rapid, and accurate prediction of the favorable tautomeric states of drug-like molecules in aqueous solution, Journal of Computer-Aided Molecular Design 24 (2010) 591–604.
[50] S. Saha, F. Wang, N–K spectra of adenine amino tautomers, Journal of Physics: Conference Series 185 (2009) 012040.
[51] W.L. Jorgensen, D.S. Maxwell, J. Tirado-Rives, Development and testing of the OPLS all-atom force field on conformational energetics and properties of organic liquids, Journal of the American Chemical Society 118 (1996) 11225–11236.
[52] A.E. Cho, D. Rinaldo, Extension of QM/MM docking and its applications to metalloproteins, Journal of Computational Chemistry 30 (2009) 2609–2616.
[53] D.W. Deerfield, C.W. Carter, L.G. Pedersen, Models for protein–zinc ion binding sites II. The catalytic sites, International Journal of Quantum Chemistry 83 (2001) 150–165.
[54] T. Dudev, C. Lim, Metal binding in proteins: the effect of the dielectric medium, Journal of Physical Chemistry B 104 (2000) 3692–3694.
[55] L. Rulíšek, Z. Havlas, Theoretical studies of metal ion selectivity. 1: DFT calculations of interaction energies of amino acid side chains with selected transition metal ions (Co^{2+}, Ni^{2+}, Cu^{2+}, Zn^{2+}, Cd^{2+}, and Hg^{2+}), Journal of the American Chemical Society 122 (2000) 10428–10439.
[56] I. Solt, N. Kulhaïnek, P.I. Simon, N. Winfield, S. Payne, M.C.G. Csaïnyi, B.M. Fuxreiter, Evaluating boundary dependent errors in QM/MM simulations, Journal of Physical Chemistry B 113 (2009) 5728–5735.
[57] V.B. Delchev, A DFT study of electron structure, geometry, and keto–enol tautomerism of 3-oxopropionyl halogenides, Monatshefte für Chemie: Chemical Monthly 135 (2004) 371–384.
[58] L. Turker, Tautomerism in 11-hydroxyaklavinone: a DFT study, Scientific World Journal 2012 (2012) 7.
[59] J. Du, H. Sun, L. Xi, J. Li, Y. Yang, H. Liu, X. Yao, Molecular modeling study of checkpoint kinase 1 inhibitors by multiple docking strategies and prime/MM–GBSA calculation, Journal of Computational Chemistry 32 (2011) 2800–2809.
[60] A.E. Cho, V. Guallar, B.J. Berne, R. Friesner, Importance of accurate charges in molecular docking: quantum mechanical/molecular mechanical (QM/MM) approach, Journal of Computational Chemistry 26 (2005) 915–931.
[61] J.M. Hayes, G. Archontis, MM-GB(PB)SA calculations of protein–ligand binding free energies, in: L. Wang (Ed.), Molecular Dynamics – Studies of Synthetic and Biological Macromolecules, InTech, Europe, 2012.
[62] D. Sitkoff, K.A. Sharp, B. Honig, Accurate calculation of hydration free energies using macroscopic solvent models, Journal of Physical Chemistry 98 (1994) 1978–1988.
[63] C. Carra, F.A. Cucinotta, Binding sites of the *E. coli* DNA recombinase protein to the ssDNA: a computational study, Journal of Biomolecular Structure and Dynamics 27 (2010) 407–427.
[64] J. Kongsted, P. Söderhjelm, U. Ryde, How accurate are continuum solvation models for drug-like molecules? Journal of Computer-Aided Molecular Design 23 (2009) 395–409.
[65] J. Kongsted, U. Ryde, An improved method to predict the entropy term with the MM/PBSA approach, Journal of Computer-Aided Molecular Design 23 (2009) 63–71.
[66] Prime version 3.0., Schrödinger, LLC, New York, NY, 2011.
[67] K. Loving, N. Salam, W. Sherman, Energetic analysis of fragment docking and application to structure-based pharmacophore hypothesis generation, Journal of Computer-Aided Molecular Design 23 (2009) 541–554.
[68] E. Yuriev, M. Agostino, P.A. Ramsland, Challenges and advances in computational docking: 2009 in review, Journal of Molecular Recognition 24 (2011) 149–164.
[69] P. Bertrand, Inside HDAC with HDAC inhibitors, European Journal of Medicinal Chemistry 45 (2010) 2095–2116.
[70] I. Schomburg, A. Chang, C. Ebeling, M. Gremse, C. Heldt, G. Huhn, D. Schomburg, BRENDA, the enzyme database: updates and major new developments, Nucleic Acids Research 32 (2004) D431–D433.
[71] D.P. Oehme, R.T.C. Brownlee, D.J.D. Wilson, Effect of atomic charge, solvation, entropy, and ligand protonation state on MM-PB(GB)SA binding energies of HIV protease, Journal of Computational Chemistry 33 (2012) 2566–2580.
[72] T. Hou, J. Wang, Y. Li, W. Wang, Assessing the performance of the MM/PBSA and MM/GBSA methods. 1: the accuracy of binding free energy calculations based on molecular dynamics simulations, Journal of Chemical Information and Modeling 51 (2010) 69–82.
[73] A. Weis, K. Katebzadeh, P. Söderhjelm, I. Nilsson, U. Ryde, Ligand affinities predicted with the MM/PBSA method: dependence on the simulation method and the force field, Journal of Medicinal Chemistry 49 (2006) 6596–6606.
[74] I. Stoica, S.K. Sadiq, P.V. Coveney, Rapid and accurate prediction of binding free energies for Saquinavir-Bound HIV-1 proteases, Journal of the American Chemical Society 130 (2008) 2639–2648.